JASA ARTICLE

Scaling laws for mitigated pile driving: Dependence of underwater noise on strike energy, pile diameter, ram weight, water depth, and mitigation system[a)]

Jonas von Pein,[1,b)] Tristan Lippert,[2] Stephan Lippert,[1] and Otto von Estorff[1]
[1]*Institute of Modelling and Computation, Hamburg University of Technology, Denickestrasse 17, 21073 Hamburg, Germany*
[2]*AQUSTIX GbR, Katharinenstrasse 4, 20457 Hamburg, Germany*

ABSTRACT:
Sound induced by impact pile driving is a possible risk to marine life. Therefore, it is common practice to use noise mitigation systems during piling to reduce the respective impact and to fulfill the prescribed noise limits. Scaling laws for the estimation of the underwater noise from unmitigated impact pile driving have been presented in von Pein, Lippert, Lippert, and von Estorff, "Scaling laws for unmitigated pile driving: Dependence of underwater noise on strike energy, pile diameter, ram weight, and water depth," Appl. Acoust. **198**, 108986 (2022). This contribution shows how these scaling laws need to be changed if noise mitigation systems are considered. Scaling laws are developed for four different kinds of noise mitigation system setups. These include big bubble curtains, double big bubble curtain combinations, a fully absorbing system directly at the pile, and the combination of a system close to the pile and a double big bubble curtain. The derived scaling laws are verified and compared to publicly available measurement data. *© 2024 Author(s). All article content, except where otherwise noted, is licensed under a Creative Commons Attribution (CC BY) license (https://creativecommons.org/licenses/by/4.0/).*
https://doi.org/10.1121/10.0030302
(Received 29 February 2024; revised 3 September 2024; accepted 10 September 2024; published online 26 September 2024)
[Editor: Stanley J Labak] Pages: 2045–2059

04 October 2024 05:14:29

I. INTRODUCTION

Piles either as monopiles or for jacket foundations are currently the most widely used foundation technique for offshore wind turbines. Offshore impact pile driving is mainly used to bring piles to the dedicated penetration depth. The pile driving process leads to the emission of very high sound levels in the water, which are potentially harmful to the marine fauna. Mammals like whales, harbor porpoises, dolphins, and seals as well as fish and other aquatic life in the ocean can change their behavior due to the high sound pressure levels or may be affected by a temporary or permanent threshold shift (compare Refs. 1–3). To protect the marine environment, limiting values have to be fulfilled in many regions of the world.[4–6] In order to estimate whether the limits will be fulfilled, precise prognosis tools are necessary. These are usually numerical[7,8] or empirical models.[9] Both have the drawback of being only available to a few experts and institutions. A common approach for scaling the sound levels for mitigated pile driving is to derive an estimate for the unmitigated case and subtract an insertion loss derived from prior measurement campaigns.[10]

An alternative way of estimating the underwater noise due to impact pile driving of steel piles is through the application of scaling laws. These can be used to scale a baseline scenario with the parameters of the future scenario. Such laws have previously been published by the authors for unmitigated impact pile driving.[11] However, in many markets, the application of noise mitigation systems (NMSs) is standard. Therefore, the dependency of the single-strike sound exposure level (SEL) on the parameters strike energy, pile diameter, water depth, and ram weight is reevaluated for cases with noise mitigation. The paper at hand can be regarded as a follow-up publication of the one published by the authors for unmitigated pile driving.[11]

Despite the SEL values at a certain position, the scaling laws can be used to derive the source levels of spreading laws, such as the Damped Cylindrical Spreading (DCS) model,[12] which has also been validated for mitigated scenarios.[13] Often, other quantities, such as the zero-to-peak pressure level SPL_{peak} are also of interest. Once the SEL is derived, the SPL_{peak} could be approximated, e.g., by the approach suggested by Heaney *et al.*[14]

The following NMSs are widely used and considered in the following: Bubble curtains are a common measure to reduce the underwater noise from offshore pile driving.[10,15] These can be deployed as a big bubble curtain (BBC), a double big bubble curtain (DBBC), or in combination with a close range system (CRS) in the direct vicinity to the pile. In the following, the dependency of the SEL on the four different parameters is investigated for a BBC, a DBBC, a fully absorbing CRS, and a combination of CRS and DBBC.

The presented results have been derived in the framework of the PhD thesis of von Pein,[16] and the scaling laws

[a)]This paper is part of a special issue on Verification and Validation of Source and Propagation Models for Underwater Sound.
[b)]Email: jonas.pein@tuhh.de

 ©Author(s) 2024.

for the BBC have partly been published by the authors in von Pein *et al.*[17,18]

This paper is organized as follows: In Sec. II, the used numerical model and the ways of including NMSs therein are briefly described and a validation of the approach with the application of a BBC is shown. The derivation of the scaling laws is shown within Sec. III. Therein, the modeled dependencies of the SEL on the parameters strike energy, pile diameter, ram weight, and water depth are shown and the physics behind the derived scaling law is explained. The scaling laws are verified against two models with different soil setups in Sec. IV and validated with a variety of mostly publicly available measurement datasets at distances of around 750 m in Sec. V. Finally, the applicability of the results and their general limits in light of the high number of uncertainties and used approximations are discussed and an outlook on future work is given.

II. NUMERICAL MODEL

The model used here is a hybrid model. It is split into a detailed close-range model and a computationally efficient far-range model. The close-range model is based on the finite element method (FEM), and it is used to derive the starting field of the Parabolic Equation (PE) far-range model. The FEM model is the same as used by von Pein *et al.*[8,11] and hence not discussed again in detail.

A. Modeling approach

The PE model is based on the split-step Padé technique as introduced by Collins,[19] which solves the outgoing part of the one-way wave equation. For the following computations, a coupling radius of 60 m is used, meaning that the pressure field obtained at 60 m with the FEM is used as the input pressure field for the PE model. The coupling radius needs to fulfill the far-field condition on which the PE theory is based. Furthermore, the coupling radius defines the lower limit of the radius of a bubble curtain in the model.

The desired quantity is the SEL defined by

$$\mathrm{SEL} = 10\log_{10}\left(\frac{E_p}{E_{p0}}\right)\left[\mathrm{dB\ re\ 1\ \mu Pa^2 s}\right], \tag{1}$$

with the sound exposure defined by $E_p = \int_{t_1}^{t_2} p^2(t)\,\mathrm{dt}$ and the reference value $E_{p0} = 1\,\mu\mathrm{Pa^2 s}$. The times t_1 and t_2 are the beginning and the end of the sound event.[20]

There are different ways to model the noise mitigation effect of an NMS. Within the FEM model, an NMS is incorporated by a mixed Dirichlet-Neumann boundary condition at the designated position of the NMS. Therefore, the modeled NMS represents a perfectly working absorbing measure and the highest possibly achievable mitigation effect is modeled. This approach is referred to as a perfectly absorbing NMS and leads to results in good agreement with measured data of the IQIP-NMS.[8,21]

The approach of a fully absorbing boundary condition leads to an overestimation of the achieved noise reduction for highly frequency-dependent noise mitigation measures, such as bubble curtains.[10,15]

In order to compute realistic results, the frequency-dependent insertion loss of the considered NMS needs to be identified. Once this is achieved, the mitigation effect can be incorporated within the PE model in the following way: A depth- and frequency-dependent transmission coefficient $T(z, f)$, which has to be derived by means of another model or by measurements, is multiplied by the pressure field modeled with the PE model at the designated position r_{NMS} of the NMS,

$$\mathrm{p}^{\star}(r_{\mathrm{NMS}}, z, f, \phi) = T(z,f)\mathrm{p}(r_{\mathrm{NMS}}, z, f, \phi). \tag{2}$$

Thereafter, the range-marching procedure of the PE model is continued with $\mathrm{p}^{\star}(r_{\mathrm{NMS}}, z, f, \phi)$ up to the next NMS or up to the dedicated final evaluation range. The profound derivation of the transmission coefficients is of great importance in order to derive reliable pile driving noise prognoses.

The approach suggested by Huisman *et al.*[22] is combining the depth-dependent reflection due to the different impedance of the air–water mixture and a first approximate of the damping induced by the resonance of the bubbles. It is based on the simplifying assumption of a constant bubble rise speed v_r and bubbles without breakup or coalescence. With v_r, the air flow per unit time per length of the nozzle hose at 1 bar Q_{atm}, and the assumption that the width of the BBC is linearly increasing with the height above the sea floor starting from the nozzle radius at the sea floor, reaching a width equal to 10% of the water depth at the sea surface, the depth-dependent volume concentration of the air can be derived. With this volume concentration $V_{\mathrm{air}}(z)$, the compressional wave speed $c_{\mathrm{mix}}(z)$ and density $\rho_{\mathrm{mix}}(z)$ of the mixed medium consisting of the mix of water and air bubbles can be calculated.[24]

With these two properties, the depth-dependent impedance $I(z) = c_{\mathrm{mix}}(z)\ \rho_{\mathrm{mix}}(z)$ and the reflection coefficient, induced by the differences in impedance, can be computed.

The way of deriving the influence of the resonance frequency on the spectral insertion loss of a bubble curtain was developed by Rolfes *et al.*,[25] applied by Huisman *et al.*,[22] and is considered in the following for the modeling procedure of the insertion loss used for the modeling of BBC and DBBC.

The first resonance frequency of the bubbles is computed with the sound speed of water c_w by

$$f_r = 0.0136\frac{c_w}{\pi d_{\mathrm{bubble}}}, \tag{3}$$

where the bubble diameter d_{bubble} is derived with respect to the dependence on the water pressure and the initial diameter of the nozzle hose. The number of bubbles can be derived by combining the depth-dependent air concentration and the depth-dependent bubble size. The respective damping per meter of the bubble curtain width is derived with the procedure described in Rolfes *et al.*[25]

The combination of the impedance and resonance-induced depth and frequency dependence is summarized in

04 October 2024 05:14:29

https://doi.org/10.1121/10.0030302

the transmission coefficient $T(z, f)$. Therein, the frequency dependence is averaged for every one-third octave band.

B. Validation of modeling approach

The majority of publications showing validations of pile driving noise models is only considering the unmitigated scenario. Validations with detailed measurement data from mitigated pile driving are sparse. Validations for cases including a DBBC are presented by von Pein *et al.*,[26] Lippert *et al.*,[27] and Peng *et al.*[28]

A detailed validation of the FEM model is shown by von Pein *et al.*[8] Therein, modeled and measured results of three sites with unmitigated pile driving are compared; and generally a good agreement is achieved. Furthermore, measurement data of two sites with mitigation measures are considered. These are a BBC and an IQIP-NMS. It is shown that a good agreement between measured and modeled data could be derived with a fully absorbing CRS close to the pile for an IQIP-NMS. For the scenario with a BBC, a slight overestimation of the mitigation potential was derived with a fully absorbing boundary condition. The same case is considered in the following with the previously described modeling approach.

The details of the considered piling configuration are taken from von Pein *et al.*[8] and Chmelnizkij *et al.*[29] These are a pile diameter of 2.48 m, a strike energy of 706 kJ, a penetration depth of 20 m, and a water depth of 40 m. The measured velocity profile is used as the pile head excitation. The considered bubble curtain parameters are a radius of 100 m, an air supply of 0.35 $m^3\,s^{-1}\,m^{-1}$, and a rise speed of 0.3 $m\,s^{-1}$. The diameter of the outlet of the hose is assumed to be 15 mm. The measurement results are taken from Bellmann *et al.*[30]

Within Fig. 1, the modeled and measured SELs are displayed over range. The modeled results have been derived with the FEM/PE model. The measured SELs agree very well with the modeled SEL being in the range of less than

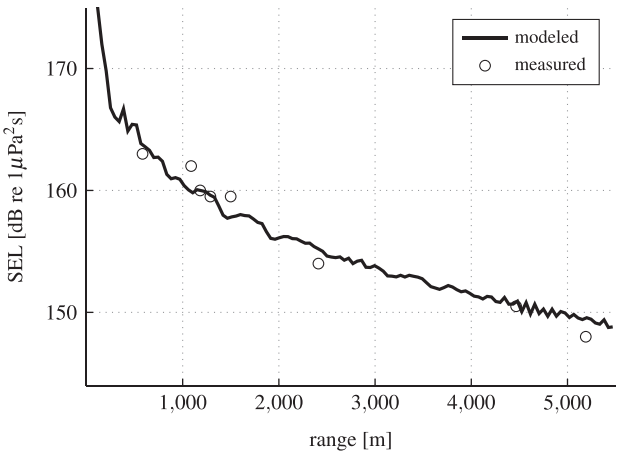

FIG. 1. Comparison of modeled and measured SELs over the range evaluated 2 m above the sea floor derived for a scenario with a BBC. The modeled results have been derived with the FEM/PE model. A pile diameter of 2.48 m, a strike energy of 706 kJ, and a water depth of 40 m are considered.

±2–3 dB, which is often referred to as measurement uncertainty.[8]

The modeling approach can be regarded as validated for pile driving noise scenarios, including a fully absorbing CRS and a BBC. Even though no validation of cases with a DBBC and a CRS/DBBC combination has explicitly been done with this specific approach, it is assumed that the model also reflects the main effects and is therefore also used for these cases to derive scaling laws for mitigated pile driving.

III. DERIVATION OF SCALING LAWS

In the following, the main influencing parameters for mitigated pile driving are identified and varied within the FEM/PE model. It has to be noted that the scaling laws assume strict linearity and neglect possible cross-interference between the considered parameters.

A. Discussion of main influencing parameters

Model runs and measurement reports indicate that, at every piling location, the emitted SELs are influenced by the interaction of various factors. These are among others: The acoustical properties and the layering of the soil, the hammer configuration, the strike energy, the pile geometry, the penetration depth, the bathymetry, the general sea state, and the use and type of noise mitigation measures.

As shown in von Pein *et al.*,[11] the main influencing parameters that are usually available with measurement reports are: The strike energy E, the pile diameter d, the ram weight m_r, and the water depth h_w. Furthermore, the type of applied NMS is usually given. The dependency of the SEL on these four parameters is evaluated with the hybrid FEM/PE model for the following NMSs: CRS, BBC, DBBC, and the combination of CRS and DBBC. It is important to note that semi-transparent CRS with a highly frequency depending insertion loss, such as the Hydro Sound Damper or the AdBm system,[10] are not considered in the following.

B. Parameter variation using the numerical model

Incorporating NMSs into the numerical investigation of the influence of different parameters on the SEL increases the number of necessary model input parameters. The frequency and depth-dependent behavior of the bubble curtains is derived with the approach described in Sec. II. A CRS is modeled as a fully absorbing system covering the whole water depth and already included within the FEM model. Therefore, in this case, all acoustical energy in the water is emitted via the soil.

The bubble curtain properties are derived with the air supply Q_{atm}, the rise speed of the bubbles v_r, and the width of the bubble curtain at the sea surface $w(h_w)$. These parameters are naturally subjected to uncertainties. Other important parameters are the distance between pile and NMS, especially for BBC and DBBC. Moreover, the application of NMSs leads to an increasing importance of the soil properties. This is due to the so-called tunneling effect, meaning

04 October 2024 05:14:29

the influence of the part of the acoustical energy, which is propagating through the soil and emitting into the water behind the NMS.

In order to take the increased number of parameters with associated uncertainties into account, model runs with several combinations of these parameters are necessary. This is done by considering real-life upper and lower bounds of the parameters and perform 50 runs with parameter combinations derived by Latin hypercube sampling.[32] The following upper and lower bounds are considered: The soil properties are varied around their nominal value within the following ranges: The compressional wave speed of the first three soil layers are in the ranges of $c_1 = [1500, 1600]$ m/s, $c_2 = [1600, 1775]$ m/s, and $c_3 = [1800, 2050]$ m/s. The corresponding thickness of these layers is varied in the ranges of $\Delta z_1 = [1, 7]$ m, $\Delta z_2 = [4, 12]$ m, and $\Delta z_3 = [5, 15]$ m. Furthermore, the damping coefficient of the first two layers is varied in the ranges of $\alpha_1 = [0.15, 0.25]$ dB/λ and $\alpha_2 = [0.3, 0.5]$ dB/λ. The damping coefficient of the third layer was set to $\alpha_3 = 0.5$ dB/λ.

The varied properties of the bubble curtains are the air supply Q_{atm}, the bubble rise speed v_r, and the width of the bubble curtain at the sea surface $w(h_w)$. These are varied in the ranges of $Q_{\text{atm}} = [0.25, 0.45]$ m^3 min^{-1} m^{-1}, $v_r = [0.25, 0.35]$ m/s, $w(h_w) = [0.08, 0.12]$ h_w. The selection of the parameters is similar to the parameters used by Huisman *et al.*[22] Another important parameter is the distance between pile and bubble curtain for a BBC. The bubble curtain radius is in the range of $r_{\text{BBC},1} = [70, 100]$ m.

For the investigation of the dependency of the sound levels on the considered parameters with the application of a DBBC, it is assumed that both bubble curtains of the DBBC have the same acoustical properties derived with the same air supply, rise speed, and width at the sea surface. The distance between the second and first bubble curtain is set to be one water depth resulting in $r_{\text{BBC},2} = h_w + r_{\text{BBC},1}$, which is a commonly applied distance. Within all variation runs including a CRS, the CRS is placed 1 m away from the pile wall.

With the 50 different parameter combinations, variation runs of the strike energy, the pile diameter, the ram weight, and the water depth are conducted for each NMS that are similar to the ones presented in von Pein *et al.*[11] and repeated for reasons of completeness.

The strike energy is varied between 500 and 8000 kJ and is conducted in the same way as described by von Pein *et al.*[11]

To reduce the number of the results, all diameter variation runs are performed with the pile head excitation derived with the impact duration of $T = 16$ ms. The lowest considered diameter is 2 m and the highest 12 m.

The ram weight variation is carried out with the pile head excitation provided by Deeks and Randolph[23] defined by

$$v(t) = v_0 \exp(-Z/m_r t), \tag{4}$$

with the pile head impedance Z and the initial velocity v_0 that can be derived out of the kinetic energy of the ram weight m_r. The ram weight is varied from 50 to 300 t.

The water depth variations are carried out for water depths ranging between 15 and 50 m.

C. Discussion of dependencies

All dependencies are evaluated at 750 m distance, and the SEL is computed as the depth-averaged sound exposure to reduce the influence of local interference effects.

The relationships between modeled parameters for mitigated scenarios differ slightly from the relationships found when modeling unmitigated scenarios.[11] For the explanation of these differences, the following highly frequency dependent factors have to be kept in mind. The soil acts as a low pass filter. Therefore, if the soil path is the main contributing source of acoustical energy in the water column, the frequency spectrum of the dominating energy is shifted toward low frequencies. This effect can also be seen in the comparison of the measurement data derived with and without the application of an IQIP-NMS in von Pein *et al.*[8] Furthermore, the bubble curtain modeling leads to lower insertion losses at low frequencies. Therefore, the application of NMSs generally leads to a greater importance of the acoustical energy emitted at lower frequencies.

In the following, the best-fit of the mean of the results of the 50 different runs is derived with the least squares method. The 50 trends are displayed after subtracting the mean of the 50 results derived with the lowest parameter. The subscript i refers to the parameter that is scaled to, while the parameters of the reference data are denoted with the subscript 0.

1. Strike energy

The results of the strike energy variation with a BBC, DBBC, CRS as well as with the combination of CRS and DBBC show similar trends as derived for the unmitigated scenario in von Pein *et al.*[11] As also shown in Fig. 2, the influence of the strike energy E can be scaled for mitigated and unmitigated scenarios by

$$\Delta \text{SEL}_{E,\text{NMS}} = 10 \log_{10}\left(\frac{E_i}{E_0}\right). \tag{5}$$

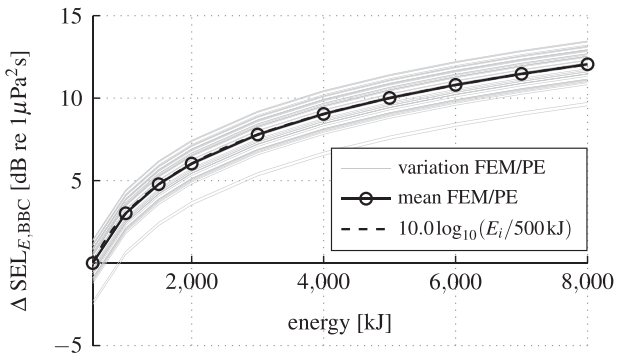

FIG. 2. Modeled dependency of the SEL on the strike energy conducted with 50 different parameter combinations evaluated and averaged over the water depth at a distance of 750 m with the application of a BBC.

04 October 2024 05:14:29

https://doi.org/10.1121/10.0030302

This is in agreement with Bellmann *et al.*,[10] who also do not distinguish between mitigated and unmitigated pile driving for the strike energy scaling.

2. Pile diameter

The modeled 50 trends, their mean, and the best-fit approximation of the diameter variation with a BBC are displayed in Fig. 3. The influence of the pile diameter d can be scaled by

$$\Delta \mathrm{SEL}_{d,\mathrm{NMS}} = k_{d,\mathrm{NMS}} \log_{10}\left(\frac{d_i}{d_0}\right) \tag{6}$$

for all NMSs. The fitted factors $k_{d,\mathrm{NMS}}$ are $k_{d,\mathrm{BBC}} = 18.3$, $k_{d,\mathrm{DBBC}} = 15.7$, $k_{d,\mathrm{CRS}} = 17.0$, and $k_{d,\mathrm{CRS/DBBC}} = 17.5$. These trends are very similar to the trend derived for unmitigated piling. However, all derived trends are slightly higher than the relation considered for unmitigated pile driving. The presence of one or more bubble curtains results in a shift of the propagating frequency spectra to lower frequencies as the BBC has a greater insertion loss at higher frequencies. An increase in pile diameter leads to a more efficient radiation at lower frequencies. The combination of these effects results in the differences in the dependencies.

All in all, the found dependencies of the SEL on the diameter for the considered mitigated scenarios are very similar. The difference between the highest and lowest fitted trends with $k_{d,\mathrm{BBC}}$ and $k_{d,\mathrm{DBBC}}$ applied to diameters ranging from 2 to 12 m is 2.0 dB, which is comparably small regarding the considered range of the varied diameter.

3. Ram weight

The results of the influence of the ram weight on the SEL modeled with a BBC are displayed in Fig. 4. Once again, a similar trend can be identified for all four considered NMSs. These can be summarized by

$$\Delta \mathrm{SEL}_{m_r} = -k_{m_r,\mathrm{NMS}} \log_{10}\left(\frac{m_{r,i}}{m_{r,0}}\right) \tag{7}$$

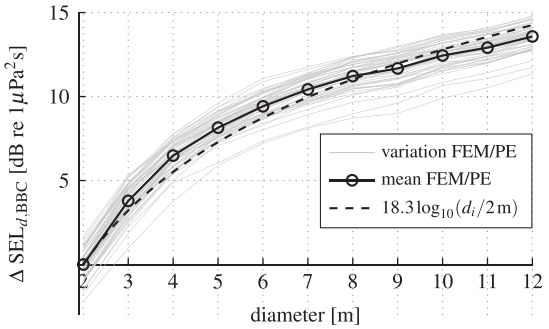

FIG. 3. Modeled dependency of the SEL on the diameter conducted with 50 different parameter combinations evaluated and averaged over the water depth at a distance of 750 m with the application of a BBC.

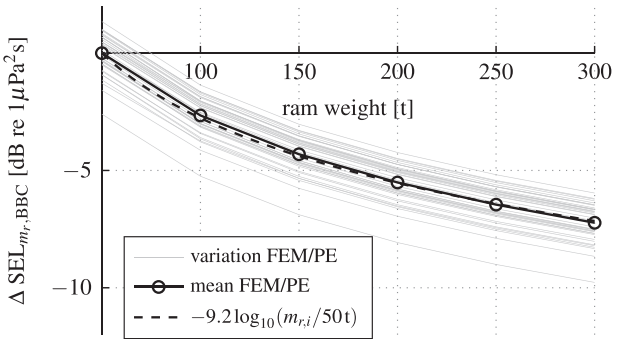

FIG. 4. Modeled dependency of the SEL on the ram weight conducted with 50 different parameter combinations evaluated and averaged over the water depth at a distance of 750 m with the application of a BBC.

with $k_{m,\mathrm{BBC}} = 9.2$. The results of the best-fit of the mean of the results for DBBC, CRS, and CRS/DBBC are $k_{m,\mathrm{DBBC}} = 8.5$, $k_{m,\mathrm{CRS}} = 6.1$, and $k_{m,\mathrm{CRS/DBBC}} = 5.4$. All trends derived for the mitigated scenarios show a lower dependence on the ram weight than the one derived for unmitigated pile driving. The differences between the $k_{m,\mathrm{NMS}}$ seem small; however, scaling with the minimal and maximal coefficient from the realistic range of 50 to 200 t already leads to a difference of up to 2.3 dB. Comparing the trends derived for BBC and DBBC as well as CRS and CRS/DBBC, it can be seen that the influence of the ram weight is decreasing with increasing number of NMSs. This is because the influence of the ram weight and the highest mitigation effect of the considered NMSs are in a similar frequency range, which is well above 100 Hz. The highest influence can be identified for the BBC followed by the DBBC. The trends are much lower for scenarios with a CRS.

As for the unmitigated case, this way of modeling is omitting the influence of a changing stiffness of the ram weight and anvil with changing hammer dimensions as well as the influence of the interaction between the hammer parts and the pile head.

4. Water depth

The dependency of the influence of the water depth on the SEL for mitigated scenarios shows the biggest difference compared to the scaling laws derived for unmitigated pile driving. The influence of the water depth on the unmitigated SEL is mainly induced by the difference in propagation loss that can be approximated with the DCS model.[12] The propagation loss of mitigated pile driving can also be estimated with the DCS as shown by Jestel *et al.*[13] However, this effect is combined with the water depth-dependent insertion loss behavior of the applied NMS.

In Fig. 5, the differences of the SEL modeled with a BBC are displayed together with resulting trend lines.

The influence of the water depth on the SEL with the application of a BBC can be approximated by a combination of the DCS with a logarithmic term. This leads to the modified DCS scaling of

04 October 2024 05:14:29

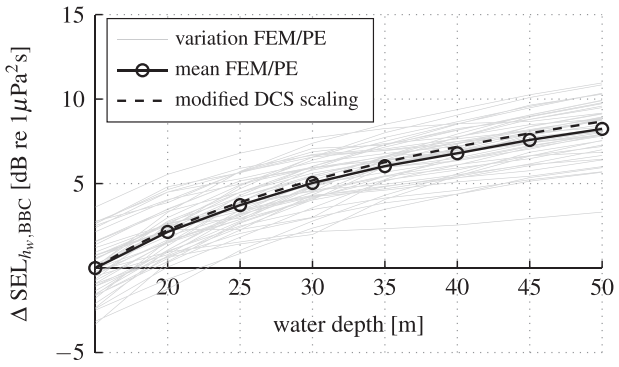

FIG. 5. Modeled dependency of the SEL on the water depth conducted with 50 different parameter combinations evaluated and averaged over the water depth at a distance of 750 m with the application of a BBC.

$$\Delta\mathrm{SEL}_{h_w,\mathrm{BBC}}(r) = \left(\frac{10\log_{10}(|R_i|^2)}{2\cot(\varphi)h_i} - \frac{10\log_{10}(|R_0|^2)}{2\cot(\varphi)h_0}\right)r + k_{h_w,\mathrm{BBC,DCS}}\log_{10}\left(\frac{h_i}{h_0}\right) \quad (8)$$

with the factor $k_{h_w,\mathrm{BBC,DCS}} = 13.9$. A simple best-fit approximation of the results at 750 m is $\Delta\mathrm{SEL}_{h_w,\mathrm{BBC}} = 16.2\log_{10}(h_i/h_0)$. The reflection coefficient R[33] used for the DCS within the fitting procedure has been derived for every individual run with the mean of the compressional wave speed of the first three soil layers and a propagation angle of $\varphi = 17°$.[34]

The trend derived for the water depth dependency of the SEL with a BBC can be qualitatively compared with the measured insertion loss, defined by the difference between the SEL measured at 750 m with and without mitigation, of Bellmann *et al.*[10] They have listed the measured insertion loss for BBCs for different water depths. To get the dependence of the insertion loss on the water depth, the water depth trend for the mitigated SEL needs to be combined with the dependence of the SEL on the water depth for the unmitigated case as provided in von Pein *et al.*[11]

Bellmann *et al.*[10] provide the following ranges of the insertion loss measured with an air flow of $Q_{\mathrm{atm}} > 0.3\,\mathrm{m^3\,min^{-1}\,m^{-1}}$: The range of the insertion loss of a BBC in water depths smaller than 25 m is between 11 and 15 dB with an averaged value of 14 dB. For water depths around 40 m, the range is between 7 and 11 dB with a mean value of 9 dB. Combining the mean values (14 and 9 dB) of the provided ranges leads to a difference of 5 dB.

For the unmitigated scenario, a difference of 0.5 dB is expected at 750 m for an increase in the water depth from 25 to 40 m.[11] Applying Eq. (8) leads to a difference of 3.3 dB. Combining these results, a difference of 3.8 dB is expected to be seen in the insertion loss, which is 1.2 dB smaller than the insertion loss derived from Bellmann *et al.*[10] Regarding the great ranges of the varied parameters ($Q_{\mathrm{atm}} = [0.25, 0.45]\,\mathrm{m^3\,min^{-1}\,m^{-1}}$) and the unknown way of how the unmitigated sound levels are derived by Bellmann *et al.*,[10] this very qualitative comparison shows a good agreement.

The modeled dependency of the SEL on the water depth derived with a DBBC is displayed in Fig. 6. Therein, the trend of the results with a DBBC can be approximated with a linear approximation

$$\Delta\mathrm{SEL}_{h_w,\mathrm{DBBC}} = k_{h_w,\mathrm{DBBC}}(h_i - h_0) \quad (9)$$

with $k_{h_w,\mathrm{DBBC}} = 0.13$.

Once again, the derived trends can be compared to the measured insertion losses provided by Bellmann *et al.*[10] The following measured ranges are provided for the application of a DBBC: For water depths below 25 m, a reduction in the range of 14 up to 18 dB with an averaged value of 17 dB and an air flow rate greater than $0.3\,\mathrm{m^3\,min^{-1}\,m^{-1}}$ is reported. For water depths around 40 m, two results are provided, which differ in the provided air flow. For an air flow rate greater than $0.3\,\mathrm{m^3\,min^{-1}\,m^{-1}}$, the broadband insertion loss reduces to ranges between 8 and 13 dB with an average of 11 dB. The difference of the two provided mean values is 6 dB. With an air flow rate greater than $0.4\,\mathrm{m^3\,min^{-1}\,m^{-1}}$, the average of the insertion loss is stated to be 15 dB. In this case, the difference is 2 dB. Therefore, the measured change in the insertion loss from the water depth of 25 m up to 40 m is in the range of 2 to 6 dB.

Applying Eq. (9) to the water depths and adding the 0.5 dB difference in propagation loss for the unmitigated scenario leads to a difference in the insertion loss of 2.5 dB. This result is in the range of the measured data.

A totally different trend of the water depth dependency can be observed for the CRS as shown in Fig. 7. Similar to the unmitigated case, the differences in the propagation loss are dominant for low water depths and can be approximated by the DCS. However, another term needs to be added to account for the following effect: Due to more energy being radiated into the water and directly absorbed by the CRS, the amount of acoustical energy tunneling the CRS is decreasing with increasing water depth. At the evaluated distance of 750 m, a maximum can be observed at 25 m in the modeled data. However, the position of the maximum depends on the considered distance. The influence of the water depth can be derived by a combination of the DCS and a linear dependence of the SEL on the water depth. A

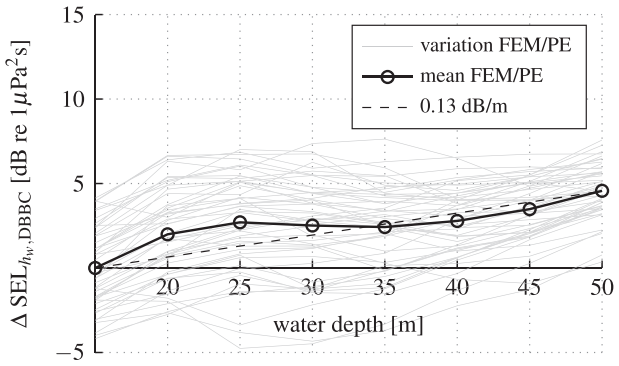

FIG. 6. Modeled dependency of the SEL on the water depth conducted with 50 different parameter combinations evaluated and averaged over the water depth at a distance of 750 m with the application of a DBBC.

04 October 2024 05:14:29

https://doi.org/10.1121/10.0030302

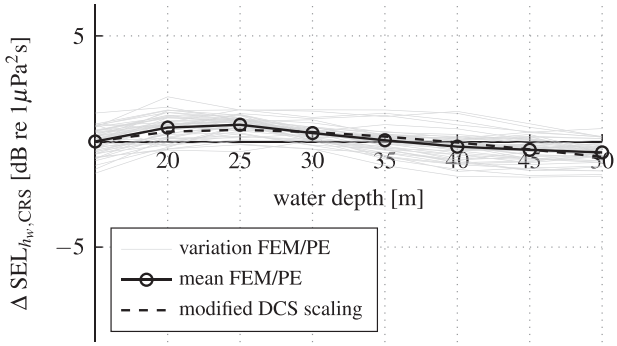

FIG. 7. Modeled dependency of the SEL on the water depth conducted with 50 different parameter combinations evaluated and averaged over the water depth at a distance of 750 m with the application of a CRS.

best-fit approximation of the linear decay term at 750 m leads to a decaying trend of about –0.1 dB/m. Further evaluations at distances close to the pile as well as further away led to similar results. Therefore,

$$\Delta\mathrm{SEL}_{h_w,\mathrm{CRS}}(r) = \left(\frac{10\log_{10}(|R_i|^2)}{2\cot(\varphi_{\mathrm{CRS}})h_i} - \frac{10\log_{10}(|R_0|^2)}{2\cot(\varphi_{\mathrm{CRS}})h_0}\right) r - 0.1(h_i - h_0) \quad (10)$$

is used for the scaling of the water depth influence with the application of a CRS.

If a perfect CRS is applied, the acoustical energy is emitted only via the soil path. Therefore, the Mach cone angle φ_{CRS} defined with the longitudinal wave speed in the pile c_p by $\sin^{-1}(c_{\mathrm{soil}}/c_{\mathrm{p}})$ is different compared to the unmitigated scenario. To derive a representative Mach cone angle for each run, the average of the compressional wave speed of the first three soil layers is considered. A simplified angle of propagation is then derived with Snell's law. The average of the run-specific propagation angles and reflection coefficients are $\varphi_{\mathrm{CRS}} = 23.2°$ and $R_{\mathrm{CRS}} = 0.96$.

The resulting dependency of the SEL on the water depth derived with the combination of a CRS and a DBBC is shown in Fig. 8. Therein it can be seen that the combination of the trends derived for a DBBC and CRS as shown in Figs. 6 and 7 leads to a good agreement with the derived results for water depths greater than 30 m. The combination of Eqs. (9) and (10) leads to

$$\Delta\mathrm{SEL}_{h_w,\mathrm{CRS/DBBC}}(r) = \left(\frac{10\log_{10}(|R_i|^2)}{2\cot(\varphi_{\mathrm{CRS}})h_i} - \frac{10\log_{10}(|R_0|^2)}{2\cot(\varphi_{\mathrm{CRS}})h_0}\right) r + 0.03(h_i - h_0). \quad (11)$$

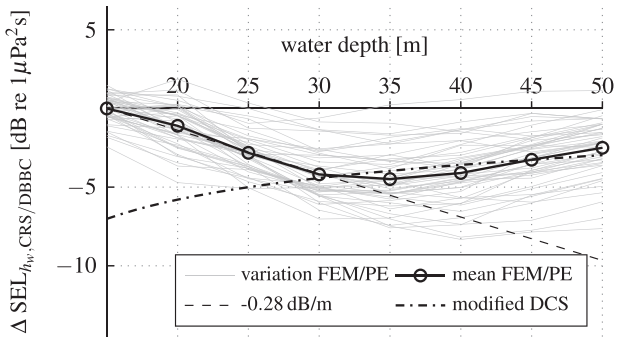

FIG. 8. Modeled dependency of the SEL on the water depth conducted with 50 different parameter combinations evaluated and averaged over the water depth at a distance of 750 m with the application of a CRS/DBBC combination.

At lower water depths, the tunneling effect is dominating the results. A simplified sketch of a characteristic ray path for a water depth of 20 and 40 m is displayed in Fig. 9. Therein it can be seen that, for smaller water depths, the acoustical energy is reflected at the sea surface and propagating back into the soil in front of the first bubble curtain. For greater water depths, the ray penetrates the bubble curtain before its first reflection at the sea floor.

The dependency of the SEL shown in Fig. 8 for water depths smaller than 30 m can be approximated by $\Delta\mathrm{SEL}_{h_w,\mathrm{CRS/DBBC}} = -0.28(h_i - h_0)$.

All in all, the dependency of the SEL on the water depth for mitigated pile driving is highly dependent on the kind of NMS. The trends derived for BBC and DBBC are comparable to provided water depth-dependent differences in the measurements of the insertion loss. Unfortunately, insertion loss data for different water depths are not available for a CRS and the combination of CRS and DBBC. Furthermore, since the influence of the water depth appears to be smaller, it would be harder to identify such trends in measured data.

IV. VERIFICATION OF SCALING LAWS

The derived scaling laws are verified in a similar manner as the scaling laws for the unmitigated scenarios described by von Pein *et al.*[11] Therein, two models are set up. The first model is based on a water depth of 20 m, a pile diameter of 3 m, a strike energy of 500 kJ, and the original geometry of the MHU 1900S hammer with a ram weight of 95 t. The second model is built up with a water depth of 40 m, a pile diameter of 6.6 m, a strike energy of 3500 kJ, and the original geometry of the MHU 3500S hammer with a ram weight of 175 t. Both piles have a wall thickness of 0.1 m and a penetration depth of 25 m is considered.

All four combinations of NMSs are verified. The CRS is modeled with a gap of 1 m between outer pile wall and the NMS. The radius of the BBC is set to 80 m, in accordance with the measurements at Global Tech I (GTI),[30] and the DBBC is modeled with an inner radius of 80 m and an outer radius of 120 m, similar to the setup described by Lippert *et al.*[27] The rise speed of the bubbles is set to $v_r = 0.3$ m/s, the air supply $Q_{\mathrm{atm}} = 0.3\,\mathrm{m^3\,min^{-1}\,m^{-1}}$, and the width at the sea surface to $w(h_w) = 0.1h_w$. The verification is conducted with the application of four different soil profiles, namely, Bard Offshore 1 (BO1), GTI, and Borkum Riffgrund 1 (BR1), all taken from von Pein *et al.*,[8] and the

04 October 2024 05:14:29

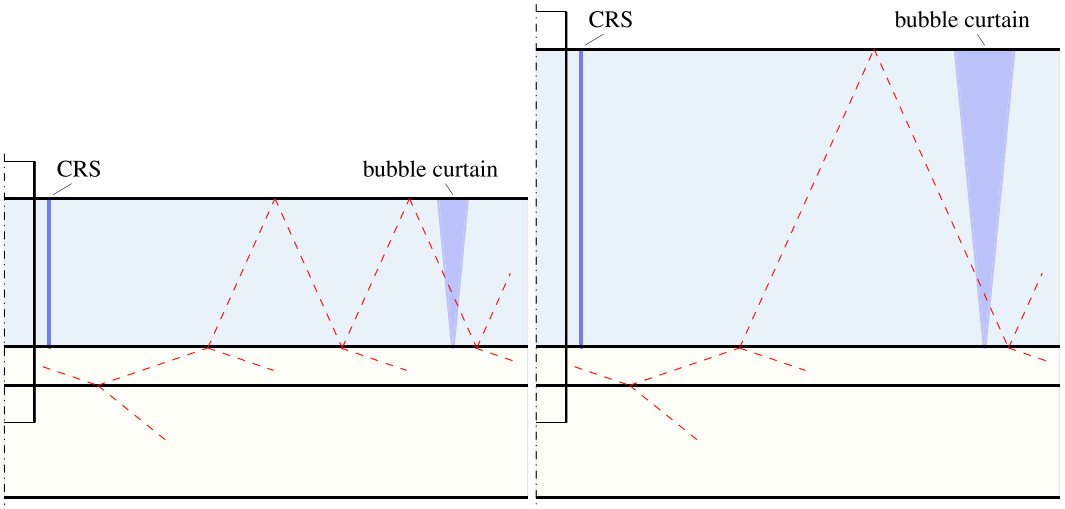

FIG. 9. (Color online) Characteristic ray paths for the combination of CRS and DBBC. The left sketch is derived for $h_w = 20$ m. The right sketch is derived for $h_w = 40$ m.

soil profile provided in the COMPILE II benchmark scenario (CPII).[31]

The verification is conducted for all four considered NMSs. The reference parameters are the ones of the first model. As previously shown, the influence of the strike energy stays the same for all scenarios. The influence of the diameter and the ram weight is considered with the best-fit results. The greatest difference for all considered NMS scenarios is the dependence on the water depth.

The scaled difference is the highest for the verification example with a BBC. This is due to the high influence of the water depth:

$$\Delta\mathrm{SEL}_{\mathrm{scaled,BBC}} = 10\log_{10}\left(\frac{E_1}{E_0}\right) + 18.3\log_{10}\left(\frac{d_1}{d_0}\right) - 9.2\log_{10}\left(\frac{m_{r,1}}{m_{r,0}}\right) + 16.2\log_{10}\left(\frac{h_1}{h_0}\right). \quad (12)$$

Therefore, the expected difference is $\Delta\mathrm{SEL}_{\mathrm{scaled,BBC}} = 17.2$ dB.

The influence of the water depth is expected to be slightly smaller if a DBBC is used. The expected difference including all varied parameters is computed by

$$\Delta\mathrm{SEL}_{\mathrm{scaled,DBBC}} = 10\log_{10}\left(\frac{E_1}{E_0}\right) + 15.7\log_{10}\left(\frac{d_1}{d_0}\right) - 8.5\log_{10}\left(\frac{m_{r,1}}{m_{r,0}}\right) + 0.13(h_1 - h_0). \quad (13)$$

With these relations, the scaled difference is $\Delta\mathrm{SEL}_{\mathrm{scaled,DBBC}} = 14.2$ dB.

The expected difference of the SEL for the CRS is computed by means of

$$\Delta\mathrm{SEL}_{\mathrm{scaled,CRS}} = 10\log_{10}\left(\frac{E_1}{E_0}\right) + 17\log_{10}\left(\frac{d_1}{d_0}\right) - 6.1\log_{10}\left(\frac{m_{r,1}}{m_{r,0}}\right) + \Delta\mathrm{SEL}_{h_{w,\mathrm{CRS}}}. \quad (14)$$

The water depth influence is $\Delta\mathrm{SEL}_{h_{w,\mathrm{CRS}}} = -1.9$ dB. It is derived by applying Eq. (10) with the propagation angle $\varphi_{\mathrm{CRS}} = 23.2$ and the reflection coefficient $R_{\mathrm{CRS}} = 0.96$. Due to the lowering influence of the water depth, the difference is the lowest of all considered mitigated scenarios. It is expected to be $\Delta\mathrm{SEL}_{\mathrm{scaled,CRS}} = 10.8$ dB.

The greatest uncertainty for the combination of CRS and DBBC is the scaling of the water depth since there is a significant variation in the results of the 50 runs (compare Fig. 8). The scaled difference of CRS/DBBC is

$$\Delta\mathrm{SEL}_{\mathrm{scaled,CRS/DBBC}} = 10\log_{10}\left(\frac{E_1}{E_0}\right) + 17.5\log_{10}\left(\frac{d_1}{d_0}\right) - 5.4\log_{10}\left(\frac{m_{r,1}}{m_{r,0}}\right) + \Delta\mathrm{SEL}_{h_{w,\mathrm{CRS/DBBC}}}. \quad (15)$$

With the water depth difference of $\Delta\mathrm{SEL}_{h_{w,\mathrm{CRS/DBBC}}} = -2$ dB derived by applying Eq. (11), the expected difference is $\Delta\mathrm{SEL}_{\mathrm{scaled,CRS/DBBC}} = 11.0$ dB.

In Table I, the modeled SELs and the resulting differences between the considered scenarios are listed and compared to the scaled difference. The highest deviation between the scaled and modeled scenarios can be found in the results derived for the CRS/DBBC combination. The averaged absolute difference is 2.8 dB. The results of the averaged difference for the other NMSs show a good agreement with 1.2 dB for the CRS, 1.1 dB for the DBBC, and 0.4 dB for the BBC. These results indicate

04 October 2024 05:14:29

https://doi.org/10.1121/10.0030302

TABLE I. Comparison of the scaled and modeled SEL at 750 m averaged over the water depth of the different scenarios with a BBC, a DBBC, a CRS, and a CRS/DBBC modeled with four different soil profiles and a penetration depth of 25 m.

Soil profile	Model	(dB re 1 μPa^2 s)	BBC	DBBC	CRS	CRS/DBBC
		ΔSEL_{scaled}	17.2	14.2	10.8	11.0
B01	Model 1	SEL	156.5	151.4	157.5	143.3
	Model 2	SEL	173.4	166.8	169.2	157.2
		$\Delta SEL_{modeled}$	16.9	15.4	11.7	13.9
GTI	Model 1	SEL	155.5	151.5	157.4	146.9
	Model 2	SEL	173.4	166.9	169.4	159.8
		$\Delta SEL_{modeled}$	17.9	15.4	12.0	12.9
BR1	Model 1	SEL	156.6	152.9	156.8	144.9
	Model 2	SEL	174.2	167.6	169.7	159.1
		$\Delta SEL_{modeled}$	17.6	14.7	12.9	14.2
CPII	Model 1	SEL	157.1	151.6	157.0	145.1
	Model 2	SEL	174.3	167.2	168.2	159.1
		$\Delta SEL_{modeled}$	17.2	15.6	11.2	14.0

the applicability of the found scaling laws for mitigated scenarios.

V. VALIDATION OF SCALING LAWS

Next, the derived scaling laws are validated against measurement datasets. First, the origin of the values and the characteristics of the piling location are described. Second, the SELs of the different piling locations are scaled and the resulting differences are compared.

A. Data used for the validation

The validation of the scaling laws for mitigated pile driving is a challenging task. On the one hand, there are only a few reports conducted with a single NMS in place; and on the other hand, the number of unknown parameters as well as their influences are expected to be even higher for mitigated piling, e.g., the local soil conditions and the bubble curtain setup and operation.

The measurement datasets used for the validation and their origin are described in the following, and the minimum and maximum values are listed in Table II.

If no water depth is provided by the data source, the water depth is retrieved from the EMODNET platform,[36] which provides bathymetry data for European waters.

The following datasets obtained from multiple pile driving locations with the application of a BBC are used for validation: Measurements of three different piles are available for the wind farm Sandbank (SB). Furthermore, data of one pile are available for the wind farms Veja Mate (VM), Trianel (TR), and Deutsche Bucht (DB). All of them were taken from the platform MarinEARS.[37] The data of two piles are available for GTI,[30] Borkum West 2 (BW2),[38] and Amrumbank West (AW).[39] The values for AW are taken from the graphs showing the sound levels over the strikes and the values close to the final penetration depth are chosen. The data of four piles of the wind farm Butendiek (BU)[40] are available.

Data of only four measurement campaigns using a DBBC were found. Lippert *et al.*[27] presented the comparison of measured and modeled SELs for skirt piles. Since the name of the site was not disclosed, this dataset is referred to as case A. At Coastal Virginia (CV) a pile was driven using a DBBC and the respective measurements are considered.[41] Furthermore, the data used for the validation of a bubble curtain modeling approach presented by Peng *et al.*[28] are considered. Once again, no site-specific name is provided. Therefore, this scenario is referred to as case B. From the Belgian part of the North Sea, the data of the Seastar wind farm (SEA)[42] are used.

It is shown by von Pein *et al.*[8] that the IQIP-NMS can be modeled as a perfectly absorbing CRS. Therefore, the scaling laws derived for the CRS are validated with measurement data conducted with an IQIP-NMS in place. Available are datasets from BR1 (Ref. 35) and BU. For the BU site the provided average of measurement results of five locations with 18 hydrophones are used.[40] Furthermore, two non-public datasets have been made available to the authors. Since the parameters cannot be published, only the scaled differences of the results are shown. These datasets are referred to as cases C and D.

The data of only two wind farms at which an IQIP-NMS/DBBC combination was used are available via MarinEARS. These are Merkur (ME) with data of 61 driven piles and Albatross (AL) with 16 measurements.

B. Validation

The validation is conducted for every considered NMS setup individually. The validity and the robustness of the validation depend on the quality and number of measurement data being publicly available. The parameters used for the validation are listed in Table II. All SELs are scaled to 750 m with the DCS prior to the validation. Data of 16 piles of eight different sites are available for the validation of scaling laws derived for the BBC.

The validation of the application of the derived scaling laws for scenarios with a DBBC and with a CRS is done by showing the difference between the scaled and actually measured results with four different datasets. The validation for the combination of CRS/DBBC is conducted the following way: Measured data of 77 piles are available from two wind farms. These datasets are scaled to one scenario with the derived scaling laws for all four parameters and plotted over the water depth.

The scaling laws validated in the following are based on Eqs. (12)–(15) in combination with the baseline SEL_0.

1. Validation for the BBC

The validation of the scaling law

04 October 2024 05:14:29

TABLE II. Ranges of the sound levels, parameters, and details of the piling configurations of the sites used for the validation of the scaling laws for mitigated offshore pile driving noise.

Wind farm	Piles (–)	SEL (dB)	Range (m)	Strike energy (kJ)	Pile diameter (m)	Water depth (m)	Ram weight (t)	Hammer type (–)	Foundation type (–)
BBC									
AW	2	161–163	750–800	1140	6	20	95	MHU 1900S	Monopile
SB	3	162–163	663–757	1013–1522	6.8	26.8–29.6	175	MHU 3500S	Monopile
VM	1	171	803	1893	7.8	39	200	Hydrohammer S4000	Monopile
TR	1	163	749	1457	8	28.3	150	Hydrohammer S3000	Monopile
DB	1	168	749	2150	8	39.3	200	Hydrohammer S4000	Monopile
BU	4	152–156	752	900	2.438	20	60	Hydrohammer S-1200	Jacket
BW2	2	160–163	750	1200	2.44	30	60	Hydrohammer S1200	Tripod
GTI	2	163–164	600–700	583	2.48	40	66	MHU 1200S	Tripod
DBBC									
A	1	159	750	2000	2.44	40	175	MHU 3500S	Jacket
CV	1	163	750	552	7.8	24	150	Hydrohammer S3000	Monopile
B	1	167	750	2150	8	40.1	200		Monopile
SEA	1	170	877	3500	8	40	200	Hydrohammer S4000	Monopile
IQIP-NMS									
BR1	1	161	738	620	5.9	27	100	Hydrohammer S2000	Monopile
BU	1	163	750	938	6	20	100	Hydrohammer S2000	Monopile
IQIP-NMS/DBBC									
AL	16	156–162	747–877	1721–2997	7.4	40.1–40.4	150	Hydrohammer S3000	Monopile
ME	61	156–160	683–752	716–2614	7.8	27.4–33.5	150	Hydrohammer S3000	Monopile

$$\mathrm{SEL}_i = \mathrm{SEL}_0 + 10\log_{10}\left(\frac{E_i}{E_0}\right) + 18.3\log_{10}\left(\frac{d_i}{d_0}\right) - 9.2\log_{10}\left(\frac{m_{r,i}}{m_{r,0}}\right) + 16.2\log_{10}\left(\frac{h_i}{h_0}\right) \quad (16)$$

derived for scenarios with a BBC by the combination of the derived trends is shown in the following.

The parameters of TR are chosen as the reference dataset for comparison. In Fig. 10, the four plots with the resulting difference between the SEL scaled with three of the four parameters and the actually measured SELs are displayed over the unscaled quantity. It can be seen that the results match very well with the derived trends, which are also plotted and intersect the minimal and maximal values. The difference between upper and lower limit of the scaling trends is between 5.9 and 7.1 dB. Furthermore, the parameters of the considered scenarios cover small diameters as typically used for skirt piles and big monopiles with diameters of up to 8 m. Accordingly, small and big hammers with the application of comparably low and high strike energies can be found in the datasets and water depth data are represented between 20 and 40 m. Comparing the standard deviation of the unscaled and scaled SEL with the application of all four scaling laws, it is reduced from 4.9 to 2.3 dB. The scaled results and the comparison to measurement data are also shown in Fig. 14. All in all, these results clearly show that the found dependencies are valid and applicable for scenarios with the application of a BBC.

2. Validation for the DBBC

In order to show that the found relations can be used for the prediction of the SEL with the application of a DBBC, the scaling law

$$\mathrm{SEL}_i = \mathrm{SEL}_0 + 10\log_{10}\left(\frac{E_i}{E_0}\right) + 15.7\log_{10}\left(\frac{d_i}{d_0}\right) - 8.5\log_{10}\left(\frac{m_{r,i}}{m_{r,0}}\right) + 0.13(h_i - h_0) \quad (17)$$

is applied to measurement data in the following. The difference between the SELs measured at SEA and the other datasets scaled to the SEA parameters with the four different derived scaling laws is displayed in Fig. 11. Therein, all scaled results agree very well with the data measured at the SEA site. The scaled measurement result of CV is overestimating the SEL by 1.4 dB. Within the measurement report, it is stated that the application of the DBBC led to smaller insertion losses than expected, which is in line with the slight overestimation. No more details of cases A and B are available. Considering the wide range of the diameter, which is between 2.44 and 8 m, the spread in strike energy ranging between 552 and 3500 kJ, and water depth combined with the multiple uncertainties related to the DBBC setup, operation, and the local soil conditions, the derived accordance between the scaled results is good. This accordance strengthens the confidence in the presented scaling laws for the DBBC; however, since only four datasets are

04 October 2024 05:14:29

https://doi.org/10.1121/10.0030302

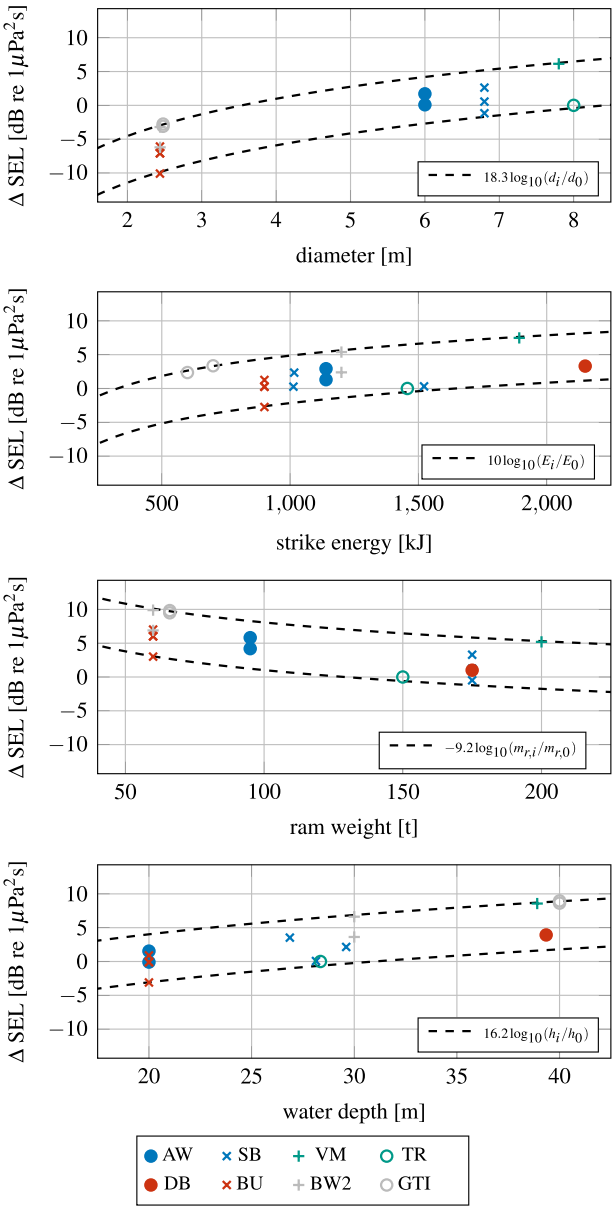

FIG. 10. (Color online) Influence of pile diameter, strike energy, ram weight, and water depth on measured SEL at 750 m with the application of a BBC. For each of the four plots, the SELs have been scaled to the parameters of the TR site, except for the parameter plotted on the x axis. The plotted value is the difference of the actual measured SEL at TR and the scaled results of the other sites.

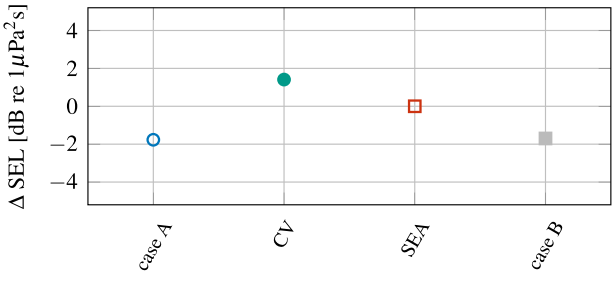

FIG. 11. (Color online) Difference between the measured and scaled results of the SEL at 750 m for all piling locations scaled with the parameters of SEA. All measurements were conducted with the application of a DBBC. All SELs are scaled to a strike energy of 3500 kJ, a pile diameter of 8 m, a ram weight of 200 t, and a water depth of 40 m.

considered, it cannot be regarded as a fully conclusive validation.

3. Validation for the CRS

The validation of the scaling law

$$\mathrm{SEL}_i = \mathrm{SEL}_0 + 10\log_{10}\left(\frac{E_i}{E_0}\right) + 17\log_{10}\left(\frac{d_i}{d_0}\right) - 6.1\log_{10}\left(\frac{m_{r,i}}{m_{r,0}}\right) + \Delta\mathrm{SEL}_{h_w,\mathrm{CRS}} \quad (18)$$

derived for cases including a CRS is conducted with the measurement data of scenarios where an IQIP-NMS system was applied. The water depth dependence $\Delta\mathrm{SEL}_{h_w,\mathrm{CRS}}$ is computed with Eq. (10). The four datasets are scaled with the strike energy, diameter, ram weight, and water depth dependencies to the parameters of BR1. The resulting difference between the scaled result of the other sites and the actual measurements of BR1 are displayed in Fig. 12. Therein, three of the four SELs agree very well with differences less than 1 dB. Only the scaled result of case D is 4 dB lower. The initial difference between the unscaled SEL is 6.5 dB. The reason for this is most likely found in the soil setup since no depth-dependent insertion loss effect is expected.

The shown comparisons of scaled and measured data are showing promising results, and strengthening the confidence in the derived scaling laws. However, since only four datasets are considered, it cannot be regarded as a fully conclusive validation.

4. Validation for CRS/DBBC

The validation of the scaling law

$$\mathrm{SEL}_i = \mathrm{SEL}_0 + 10\log_{10}\left(\frac{E_i}{E_0}\right) + 17.5\log_{10}\left(\frac{d_i}{d_0}\right) - 5.4\log_{10}\left(\frac{m_{r,i}}{m_{r,0}}\right) + \Delta\mathrm{SEL}_{h_w,\mathrm{CRS/DBBC}} \quad (19)$$

is conducted as follows:

Since the available measurement data have been measured at locations with water depths greater than 27 m, the

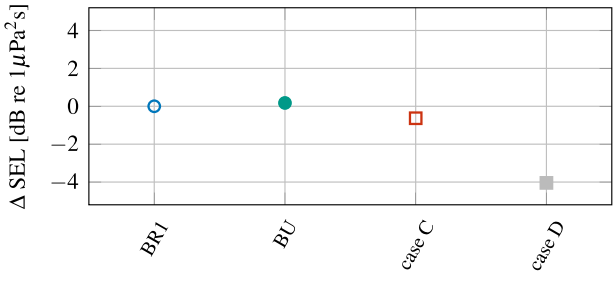

FIG. 12. (Color online) Difference between the measured and scaled results of the SEL at 750 m for all piling locations scaled with the parameters of BR1. All measurements were conducted with the application of an IQIP-NMS. All SELs are scaled to a strike energy of 620 kJ, a pile diameter of 5.9 m, a ram weight of 100 t, and a water depth of 27 m.

04 October 2024 05:14:29

influence of the water depth $\Delta SEL_{h_{w,CRS/DBBC}}$ is scaled with Eq. (11).

Two datasets of wind farms at which the SEL was measured during the application of the combination of an IQIP-NMS and a DBBC are available. As listed in Table II, the variation of the parameters is rather small.

In the following, all datasets are scaled to the parameters of ME. These are the average of the applied strike energy 1868 kJ, a pile diameter of 7.4 m, and an averaged water depth of 30.4 m. The same hammer type has been used for both wind farms.

The mean of the measured values without scaling is 158.4 dB for ME and 159.3 dB for AL. The influence of the diameter is about 0.4 dB. The combined scaling of strike energy and diameter leads to an average of 158.5 dB for ME and 158.6 dB for AL. The application of the water depth scaling leads to the averages of 158.5 dB for ME and 157.9 dB for AL. When comparing these differences, it is important to keep in mind that the original measurement data did not include decimal places.

The measurement data of ME and AL scaled to the mean strike energy of ME, the diameter of ME, and the average water depth of ME are displayed over the water depth in Fig. 13. Therein, the range between the highest and lowest scaled SEL of each wind farm is 8.6 dB for ME and 6.5 dB for AL. These comparably high ranges are resulting out of the differences within the local soil conditions and presumably in the pile specific bubble curtain setup and operation.

The comparison shows the advantages and the limits of the approach of scaling the SEL from one to another. The scaling of the SEL leads to a good agreement of the averaged SELs of the different sites. However, a spread in the scaled data remains. This spread could be slightly reduced with more detailed scaling laws, such as taking the air supply, the bubble curtain radii, and measurement conditions into account. However, the remaining measurement uncertainties, soil conditions, and real-life bubble curtain performance will always lead to a certain range in the measurements derived in a single wind farm.

The presented results indicate the possible usage of the derived scaling laws for the CRS/DBBC combination. However, the available database only covers a small range of the parameters. Therefore, further data for a sufficient validation are necessary.

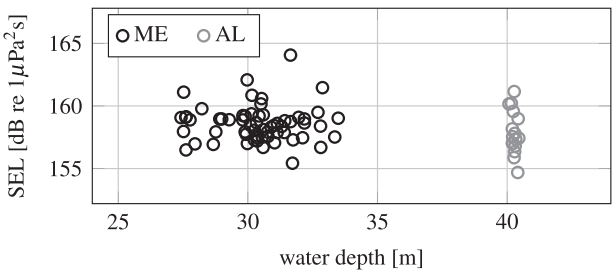

FIG. 13. Comparison of the scaled SELs over the water depth with the application of the combination IQIP-NMS/DBBC of ME and AL scaled to the parameters of ME. All SELs are scaled to a strike energy of 1868 kJ, a pile diameter of 7.8 m, and a water depth of 30.4 m.

VI. DISCUSSION

The derived scaling laws for the SEL of mitigated pile driving mainly differ in their NMS-specific dependence on the water depth.

The differences in the dependency of the SEL for the different NMSs on the diameter and the ram weight are rather small, however, indicating explainable trends, such as a higher ram weight leading to a reduction in a similar frequency range and therefore leading to a slightly smaller reduction of the sound levels. The application of the considered NMSs led to a change in the emitted spectrum with a shift to lower frequencies. This is also demonstrated by Bellmann *et al.*[10] who show that the insertion loss of all considered systems increases with frequency. The reduction effect of the increase in the ram weight, with the considered simplified pile head excitation model, is highest above 100 Hz. The change to a hammer with a heavier ram weight can also lead to local shifts in the frequency spectrum due to the differences in the pile head excitation spectrum. The pile head excitation is, of course, also influenced by the stiffness of the hammer components, which are neglected in the derivation of the dependency of the SEL on the ram weight. The local shifts in the underwater noise spectrum can be seen at frequencies below 100 Hz in Bellmann *et al.*[10] (their Fig. 21) and in the pile head excitations of BR1 and CPII von Pein *et al.*[11] (their Fig. 3). The difference between the ram weight scaling from 100 to 200 t with the BBC scaling law and the CRS/DBBC scaling law is 1.1 dB. This is in the range of measurement uncertainties, especially since the majority of the measurement data are provided without decimal places. Therefore, these small differences cannot easily be validated.

Comparing the differences between the upper and lower trend lines of the BBC results of the SEL in Fig. 10, a similar margin as for the unmitigated scenarios[11] can be identified. This outcome is rather unexpected, since the influence of not included parameters was expected to be higher compared to the unmitigated cases. These are, if bubble curtains are used, their radii, the air supply, the design, the operation, the depth and frequency-dependent behavior of the bubble curtain, in combination with a greater importance of the soil parameters. The soil properties are expected to gain even higher importance due to tunneling effects. However, investigations of the influence of soil parameters have mainly been published for unmitigated pile driving scenarios.[43]

In addition to the mentioned parameters, the efficiency of the bubble curtain is also relying on the flow speed of the water.

A common approach for scaling the sound levels for mitigated pile driving is to derive an estimate for the unmitigated case and subtract an insertion loss derived by several measurement campaigns.[10] The presented scaling laws for mitigated pile driving allow for a direct estimation of the

04 October 2024 05:14:29

https://doi.org/10.1121/10.0030302

SELs for mitigated scenarios. This is done for the sites at which measurement data with and without a BBC are available. The measured and estimated SELs of the sites at which pile driving was conducted with and without a BBC are displayed in Fig. 14. Therein, the statistical evaluation of the scaled results is shown with boxplots that indicate the mean, the upper and lower quartile as well as the minimum and maximum values of the scaled measurement data. The results of the unmitigated scenarios are derived with the scaling of 20 of the 21 measurement datasets as provided by von Pein *et al.*,[11] and the scaled results with the application of a BBC are derived by scaling the data from 7 of the 8 sites from Table II. Furthermore, the SEL derived by subtracting a water depth-dependent insertion loss from the scaled result of the unmitigated scenario is shown with crossed-whisker plots. The applied insertion loss is taken from Ref. 10 and is 14 dB for water depths smaller than 25 m, 11 dB for water depths around 30 m, and 9 dB for water depths around 40 m. Ranges of ±3 dB for the water depths of 25 and 30 m as well as ±2 dB for water depths around 40 m are also provided. The dots denote measured values. The measured results of the unmitigated and mitigated cases of BU have been obtained with piles of different diameter. Therefore, no SEL derived with the application of the insertion loss is provided for this case.

The scaled results generally agree well with the measurement data, and the application of the measured insertion loss leads to similar results. The range between upper and lower quartile is very similar for the SEL with and without a BBC. This way of comparing the datasets also allows new insights into the actual NMS performance by comparing the mitigated and unmitigated sound levels with other measurement data. This procedure allows one to see whether the unmitigated and mitigated sound levels are uncommonly high or low. For example, if only the measured values of the SB site with and without the BBC are compared, the BBC performance seems to be very good. However, the unmitigated sound levels of the SB site are the highest in the dataset, while the sound levels measured with the application of a BBC are well comparable to the scaled results of the other sites. Therefore, the scaled results show that a good BBC performance is achieved; and at the same time, the unmitigated sound levels are uncommonly high. The measured and scaled results of VM show an opposite result. The unmitigated sound levels are well in the range of the other datasets, and the mitigated sound levels are at the upper end of the range of the compared data.

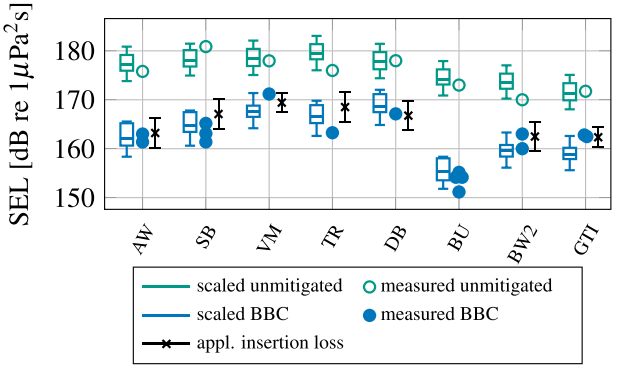

FIG. 14. (Color online) Comparison of the measured and scaled ranges of the SEL with and without the application of a BBC.

Another example is the comparison of the measured sound levels of TR. There, the mitigated as well as the unmitigated SELs are at the lower range of the estimations, which indicates that other factors led to a comparably silent scenario.

The application of the found dependencies for the scaling of the SEL with the application of a perfect CRS, a DBBC, and their combination also shows a good agreement between scaled and measured SELs, especially if measurement errors and typical variations within one site are taken into account. Even though not enough measurement data are available to conduct a decent validation, the displayed comparisons strengthen the confidence in the applicability of the derived scaling laws. Once further data are available, a statistical evaluation of the scaled results as conducted in Fig. 14 is suggested in order to derive a range of the estimate. Moreover, it must be emphasized that the CRS in the model was considered as a fully absorbing system and the validation was performed with data derived with an existing IQIP-NMS. Semi-transparent CRSs with a strongly frequency-dependent insertion behavior were not considered in the paper at hand.

VII. CONCLUSION AND OUTLOOK

Simple to apply scaling laws for four different kinds of noise mitigation measures are developed within this paper. The dependencies of the SEL on the strike energy, the pile diameter, the ram weight, and the water depth are derived for four different representative NMS setups, which are BBC, DBBC, CRS, and CRS/DBBC. A detailed validation with data from 16 piles from eight sites is conducted for scenarios with the application of a BBC. The conducted validation is showing similar differences between upper and lower bounds as derived for unmitigated scenarios in a previous publication. Due to the higher number of uncertain parameters and simplifications made, this outcome was not expected.

More data are necessary for the validation of the found scaling laws for scenarios with a DBBC, CRS, and CRS/DBBC to achieve a reliable validation. However, the conducted comparisons already increase the confidence in the derived scaling laws being able to scale the SEL.

The application of the estimations to scenarios with and without a BBC show that these scaling laws allow more insight into the actual performance of an NMS.

The comparisons of the scaled measurement data for the IQIP-NMS/DBBC sites indicate that the scaling laws can only perform as well as the baseline prediction and the quality of the measurements allow them to do. The application of the scaling laws leads to a reduction of the span of variation within the sound levels of a single wind farm. The

04 October 2024 05:14:29

remaining variation within a site needs to be considered and identified if it is related to, e.g., the DBBC operation, soil conditions, or measurement errors.

All in all, the found scaling laws can never improve a bad baseline prediction or measurement. Therefore, care needs to be taken when choosing such. Furthermore, a case by case evaluation of the pros and cons of the use of a scaling law and the additional use of numerical models should be done. Significant differences in the soil conditions, pile design, hammer type, and NMS setup could make additional model runs necessary.

The next steps will be to use more measurement data to conduct validations for a greater parameter range and to investigate the application for non-perfectly working CRS.

ACKNOWLEDGMENTS

We would like to thank the industrial partner MENCK for their support and the fruitful cooperation.

AUTHOR DECLARATIONS

Conflict of Interest

There are no conflicts of interest to declare.

DATA AVAILABILITY

The data that support the findings of this study are available from the corresponding author upon reasonable request.

[1]R. A. Kastelein, R. Gransier, M. A. T. Marijt, and L. Hoek, "Hearing frequency thresholds of harbor porpoises (*Phocoena phocoena*) temporarily affected by played back offshore pile driving sounds," J. Acoust. Soc. Am. **137**(2), 556–564 (2015).

[2]A. N. Popper, L. Hice-Dunton, E. Jenkins, D. M. Higgs, J. Krebs, A. Mooney, A. Rice, L. Roberts, F. Thomsen, K. Vigness-Raposa, D. Zeddies, and K. A. Williams, "Offshore wind energy development: Research priorities for sound and vibration effects on fishes and aquatic invertebrates," J. Acoust. Soc. Am. **151**(1), 205–215 (2022).

[3]E. B. L. Southall, J. J. Finneran, C. Reichmuth, P. E. Nachtigall, D. R. Ketten, A. E. Bowles, W. T. Ellison, D. P. Nowacek, and P. L. Tyack, "Marine mammal noise exposure criteria: Updated scientific recommendations for residual hearing effects," Aquat. Mamm. **45**(2), 125–232 (2019).

[4]A. Müller and C. Zerbs, "Offshore wind farms prediction of underwater sound minimum requirements on documentation," Technical Report, Federal Maritime and Hydrographic Agency (BSH), Hamburg, Germany (2013).

[5]National Marine Fisheries Service, "Technical guidance for assessing the effects of anthropogenic sound on marine mammal hearing (version 2.0, revision)," National Marine Fisheries Service, Silver Spring, MD (2018), p. 167.

[6]Danish Energy Agency, "Guideline for underwater noise: Installation of impact or vibratory driven piles," Danish Energy Agency, Copenhagen, Denmark (2022).

[7]S. Lippert, M. Nijhof, T. Lippert, D. Wilkes, A. Gavrilov, K. Heitmann, M. Ruhnau, O. von Estorff, A. Schäfke, I. Schäfer, J. Ehrlich, A. MacGillivray, J. Park, W. Seong, M. A. Ainslie, C. De Jong, M. Wood, L. Wang, and P. Theobald, "COMPILE: A generic benchmark case for predictions of marine pile-driving noise," IEEE J. Oceanic Eng. **41**(4), 1061–1071 (2016).

[8]J. von Pein, S. Lippert, and O. von Estorff, "Validation of a finite element modelling approach for mitigated and unmitigated pile driving noise prognosis," J. Acoust. Soc. Am. **149**(3), 1737–1748 (2021).

[9]S. Gründert, S. van de Par, and M. A. Bellmann, "Empirische Modellierung zur Prädiktion von Hydroschallimmissionen bei Impulsrammung von Fundamentstrukturen für Offshore-Windenergieanlagen" ("Empirical modeling for prediction of hydro-sound immissions during impulse pile driving of foundation structures for offshore wind turbines"), in *Proceedings of DAGA 2014*, Oldenburg, Germany (2014), pp. 449–450.

[10]M. A. Bellmann, A. May, T. Wendt, S. Gerlach, and P. Remmers, "Underwater noise during the impulse pile-driving procedure: Influencing factors on pile-driving noise and technical possibilities to comply with noise mitigation values," Technical Report (2020), available at https://www.itap.de/media/experience_report_underwater_era-report.pdf.

[11]J. von Pein, T. Lippert, S. Lippert, and O. von Estorff, "Scaling laws for unmitigated pile driving: Dependence of underwater noise on strike energy, pile diameter, ram weight, and water depth," Appl. Acoust. **198**, 108986 (2022).

[12]T. Lippert, M. A. Ainslie, and O. von Estorff, "Pile driving acoustics made simple: Damped cylindrical spreading model," J. Acoust. Soc. Am. **143**(1), 310–317 (2018).

[13]J. Jestel, J. von Pein, T. Lippert, and O. von Estorff, "Damped cylindrical spreading model: Estimation of mitigated pile driving noise levels," Appl. Acoust. **184**, 108350 (2021).

[14]K. D. Heaney, M. A. Ainslie, M. B. Halsvorsen, K. D. Seger, R. A. J. Müller, M. J. J. Nijhof, and T. Lippert, "A parametric analysis and sensitivity study of the acoustic propagation for renewable energy sources," OCS Study BOEM 2020-011, U.S. Department of the Interior, Bureau of Ocean Energy Management (CSA Ocean Sciences Inc., Washington, DC, 2020) 165 pp.

[15]S. Koschinski and K. Lüdemann, "Noise mitigation for the construction of increasingly large offshore wind turbines: Technical options for complying with noise limits," Technical Report, Federal Agency for Nature Conservation, Bonn, Germany (2020).

[16]J. von Pein, "Scaling laws for offshore pile driving noise and bathymetry induced 3D effects," Ph.D. thesis, Shaker Verlag, Düren, Germany, 2024.

[17]J. von Pein, T. Lippert, S. Lippert, and O. von Estorff, "Scaling offshore pile driving noise: Estimating the relevant sound pressure levels," in *Proceedings of the International Congress on Acoustics*, Gyeongju, Korea (2022).

[18]J. von Pein, T. Lippert, S. Lippert, and O. von Estorff, "Scaling offshore pile driving noise: Examples for scenarios with and without a big bubble curtain," Proc. Mtgs. Acoust. **47**, 070015 (2022).

[19]M. D. Collins, "A split-step Padé solution for the parabolic equation method," J. Acoust. Soc. Am. **93**(4), 1736–1742 (1992).

[20]DIN ISO18406:2018-08, "Underwater acoustics: Measurement of radiated underwater sound from percussive pile driving (ISO 18406:2017)" (International Organization for Standardization, Geneva, Switzerland, 2018).

[21]K. Heitmann, M. Ruhnau, T. Lippert, S. Lippert, and O. von Estorff, "Numerical investigation of the influence of different sound mitigation systems on the underwater sound pressure level due to offshore pile driving," in *Proceedings of ICSV 2015*, Florence, Italy (2015).

[22]M. Huisman, L. Lederwasch, and R. Smidt Lützen, "Bubble curtain modelling: Analytical prediction of underwater piling noise mitigation," in *Proceedings of Inter-Noise 2021*, Washington, DC (2021).

[23]A. J. Deeks and M. F. Randolph, "Analytical modelling of hammer impact for pile driving," Numer. Anal. Methods Geomech. **17**, 279–302 (1993).

[24]H. Grandjean, "Propagation d'une onde de choc dans un liquide aéré: Modélisation et application aux rideaux de bulles" ("Shock wave propagation in an aerated liquid: Modelling and application to bubble curtains"), Ph.D. thesis, Université de Bretagne Occidentale, Brest, France, 2012.

[25]R. Rolfes, J. Rustemeier, M. Neuber, T. Grießmann, A. Ewaldt, A. Uhl, M. S.-v. Glahn, K. Betke, R. Matuschek, and A. Lübben, "Konzeption, Erprobung, Realisierung und Überprüfung von lärmarmen Bauverfahren und Lärmminderungsmaßnahmen bei der Gründung von Offshore-WEA (Schall 3)" ("Design, testing, implementation and verification of low-noise construction methods and noise abatement systems for offshore foundations"), Technical Report, Universität Hannover, Hannover, Germany (2012).

[26]J. von Pein, S. Lippert, and O. von Estorff, "Validation of a 3D pile driving noise model with noise mitigation measures," in *6th Underwater Acoustics Conference and Exhibition* (2021), Vol. 44, p. 070014.

04 October 2024 05:14:29

[27]S. Lippert, M. Huisman, M. Ruhnau, O. von Estorff, and K. van Zandwijk, "Prognosis of underwater pile driving noise for submerged skirt piles of jacket structures," in *Proceedings of the UACE 2017 4th Underwater Acoustics Conference and Exhibition*, Skiathos, Greece (2017).
[28]Y. Peng, A. Tsouvalas, T. Stampoultzoglou, and A. Metrikine, "Study of the sound escape with the use of an air bubble curtain in offshore pile driving," J. Mar. Sci. Eng. **9**(2), 232 (2021).
[29]A. Chmelnizkij, O. von Estorff, J. Grabe, E. Heins, K. Heitmann, S. Lippert, T. Lippert, M. Ruhnau, K. Siegl, T. Bohne, T. Grießmann, R. Rolfes, J. Rustemeier, C. Podolski, W. Rabbel, and D. Wilken, "Schlussbericht des Verbundprojektes BORA: Entwicklung eines Berechnungsmodells zur Vorhersage des Unterwasserschalls bei Rammarbeiten zur Gründung von OWEA" ("Final Report of the Research Project BORA: Development of a prediction model for underwater noise caused by pile driving for offshore wind farms"), Technical Report, Hamburg University of Technology, Institute of Modelling and Computation, Institute of Geotechnical Engineering and Construction Management; Leibniz University Hannover, Institute of Structural Analysis; Kiel University, Christian-Albrechts-Universität, Hamburg, Germany (2016).
[30]M. A. Bellmann, S. Gündert, and P. Remmers, "Offshore Messkampagne 2 (OMK2) für das Projekt BORA im Offshore-Windpark Global Tech I" ["Offshore measurement campaign 2 (OMK2) for the BORA project at the wind farm Global Tech I"], Technical Report (2015).
[31]S. Lippert, O. von Estorff, M. Nijhof, and T. Lippert, "COMPILE II: A benchmark of pile driving noise models against offshore measurements," in *Proceedings of Inter-Noise 2018*, Chicago (2018).
[32]M. D. McKay, R. J. Beckman, and W. J. Conover, "A comparison of three methods for selecting values of input variables in the analysis of output from a computer code," Technometrics **42**(1), 55–61 (2000).
[33]C. T. Tindle and Z. Y. Zhang, "An equivalent fluid approximation for a low shear speed ocean bottom," J. Acoust. Soc. Am. **91**(6), 3248–3256 (1992).
[34]P. G. Reinhall and P. H. Dahl, "Underwater Mach wave radiation from impact pile driving: Theory and observation," J. Acoust. Soc. Am. **130**(3), 1209–1216 (2011).
[35]M. A. Bellmann, S. Gündert, and P. Remmers, "Offshore Messkampagne 3 (OMK3) für das Projekt BORA im Offshore-Windpark Borkum Riffgrund 01" ["Offshore measurement campaign 3 (OMK3) for the BORA project at the wind farm Borkum Riffgrund 01"], Technical Report (2015).
[36]European Marine Observation and Data Network (EMODNet) (2022), available at https://portal.emodnet-bathymetry.eu/.
[37]MarinEARS: Marine Explorer and Registry of Sound: specialist information system for underwater noise and national noise-register for the notification of impulsive noise events in the German EEZ of the North- and Baltic Sea to the EU according to the MSF (2022), available at https://marinears.bsh.de.
[38]A. Diederichs, H. Pehlke, G. Nehls, M. Bellmann, P. Gerke, J. Oldeland, C. Grunau, S. Witte, and A. Rose, "Entwicklung und Erprobung des Großen Blasenschleiers zur Minderung der Hydroschallemissionen bei Offshore-Rammarbeiten" ("Development and testing of the Big Bubble Curtain to reduce hydro-acoustic emissions during offshore pile driving"), Technical Report, Husum, Germany (2014).
[39]P. Stein, H. Sychla, B. Bruns, C. Kuhn, J. Gattermann, and J. Stahlmann, "Evaluierung von zwei gemeinsam eingesetzten Schallminderungsmaßnahmen (HSD und BBC) bei den Monopile-Gründungen im OWP Amrumbank West: Untersuchung der Schallkopplungen zwischen Pfahl, Boden und Wasser" ["Evaluation of two jointly applied noise mitigation measures (HSD and BBC) at the monopile foundations in the Amrumbank West OWP: Investigation of the noise couplings between pile, soil and water"], Technical Report, Braunschweig, Germany (2016).
[40]H. Holst and M. A. Bellmann, "Offshore-Windpark Butendiek Baumonitoring Marine Säuger Hydroschallmessungen" ("Offshore wind farm Butendiek Construction monitoring Marine mammals Hydro sound measurements"), Technical Report (2014).
[41]J. Brinkkemper, "Coastal Virginia offshore wind: Noise monitoring during monopile installation A01 and A02," Technical Report (2020), available at https://tethys.pnnl.gov/sites/default/files/publications/coastal_virginia_offshore_wind_final_noise_and_pso_monitoring_report.pdf.
[42]A. Norro, "An evaluation of the noise mitigation achieved using double big bubble curtains in offshore pile driving in the southern North Sea," Memoirs on the Marine Environment (2020).
[43]T. Lippert and O. von Estorff, "The significance of parameter uncertainties for the prediction of offshore pile driving noise," J. Acoust. Soc. Am. **136**(5), 2463–2471 (2014).

04 October 2024 05:14:29